GFZ
Helmholtz-Zentrum
POTSDAM

Originally published as:

Zhu, C., Cotton, F., Pilz, M. (2019): Testing the Depths to 1.0 and 2.5 km/s Velocity Isosurfaces in a Velocity Model for Japan and Implications for Ground-Motion Modeling. - *Bulletin of the Seismological Society of America*, *109*, 6, pp. 2710—2721.

DOI: http://doi.org/10.1785/0120190016

Bulletin of the Seismological Society of America, Vol. XX, No. XX, pp. –, – 2019, doi: 10.1785/0120190016

Testing the Depths to 1.0 and 2.5 km/s Velocity Isosurfaces in a Velocity Model for Japan and Implications for Ground-Motion Modeling

by Chuanbin Zhu, Fabrice Cotton,* and Marco Pilz

Abstract In the Next Generation Attenuation West2 (NGA-West2) project, a 3D subsurface structure model (Japan Seismic Hazard Information Station [J-SHIS]) was queried to establish depths to 1.0 and 2.5 km/s velocity isosurfaces for sites without depth measurement in Japan. In this article, we evaluate the depth parameters in the J-SHIS velocity model by comparing them with their corresponding site-specific depth measurements derived from selected KiK-net velocity profiles. The comparison indicates that the J-SHIS model underestimates site depths at shallow sites and overestimates depths at deep sites. Similar issues were also identified in the southern California basin model. Our results also show that these underestimations and overestimations have a potentially significant impact on ground-motion prediction using NGA-West2 ground-motion models (GMMs). Site resonant period may be considered as an alternative to depth parameter in the site term of a GMM.

Introduction

Many ground-motion models (GMMs) use the time-averaged shear-wave velocity in the upper 30 m (V_{S30}) as the sole proxy to parameterize a site (e.g., Douglas, 2011). However, V_{S30} alone is not adequate to capture all the site effects, especially at long spectral periods ($> \sim 1.0$ s), because at long periods, one-fourth of its wavelengths may exceed 30 m, and thus ground motion would be controlled more by deep and large-scale seismic velocity structures than by the sediments within the first 30 m.

To improve the ground-motion estimation at long periods, a depth parameter Z_x (the depth to a shear-wave isosurface having $V_S = x$ km/s), in addition to V_{S30}, is considered in many studies (Pitilakis *et al.*, 2013). For the Next Generation Attenuation project (NGA-West2, Table 1), whereas Abrahamson *et al.* (2014; hereafter, ASK14), Boore *et al.* (2014; hereafter, BSSA14), and Chiou and Youngs (2014; hereafter, CY14) used $Z_{1.0}$ in their site terms, Campbell and Bozorgnia (2014; hereafter, CB14) opted for $Z_{2.5}$. Most of these depth parameters were obtained from regional velocity structure models (Graves and Aagaard, 2011; Ancheta *et al.*, 2014), that is, the Community Velocity Model-S4 (CVM-S4) (Magistrale *et al.*, 2000) and CVM-H1.1.0 (Süss and Shaw, 2003) basin models for southern California, 3D velocity model of the bay area (Boatwright *et al.*, 2004) for northern California, and the Japan Seismic Hazard Information Station (J-SHIS) model (Fujiwara *et al.*, 2009) for Japan.

Quality of site data is of great significance for empirical studies on site effects. Stewart *et al.* (2005) investigated the bias of southern California basin depth parameters (Magistrale *et al.*, 2000), which were found to have an underestimation bias near the basin margin and overestimation bias near the middle of the basin. The J-SHIS velocity model was queried to establish depth database for sites without depth measurements to 1.0 and 2.5 km/s in Japan during the NGA-West2 project. It is thus important to test the J-SHIS depths and evaluate the impact of potential underestimations or overestimations on NGA-West2 GMMs.

In this study, we first identify KiK-net sites with useable borehole logging data following a stringent procedure. From these velocity profiles, we obtain site-specific depth measurements and then compare them with depths extracted from the J-SHIS model. Then we discuss the implications of the identified depth differences on V_{S30}-depth centering and on ground-motion estimation using NGA-West2 GMMs.

J-SHIS Subsurface Structure Model

The J-SHIS model is a 3D subsurface structure model for Japan (see Data and Resources). It was developed by the National Research Institute for Earth Science and Disaster Prevention (NIED). The 3D structure of the J-SHIS model was determined based on results of various structural explorations (e.g., velocity logging, reflection and refraction surveys, microtremor surveys, and gravity surveys) and geological information (e.g., topographical maps, geological maps and sections, and boring column diagrams). Then the model depths were modified to match the dominant period of

*Also at Institute for Earth and Environmental Sciences, University of Potsdam, Karl-Liebknecht-Straße 24-25, 14476 Potsdam, Germany.

Downloaded from https://pubs.geoscienceworld.org/ssa/bssa/article-pdf/doi/10.1785/0120190016/4832689/bssa-2019016.1.pdf
by GeoForschungsZentrums Potsdam, Chuanbin Zhu

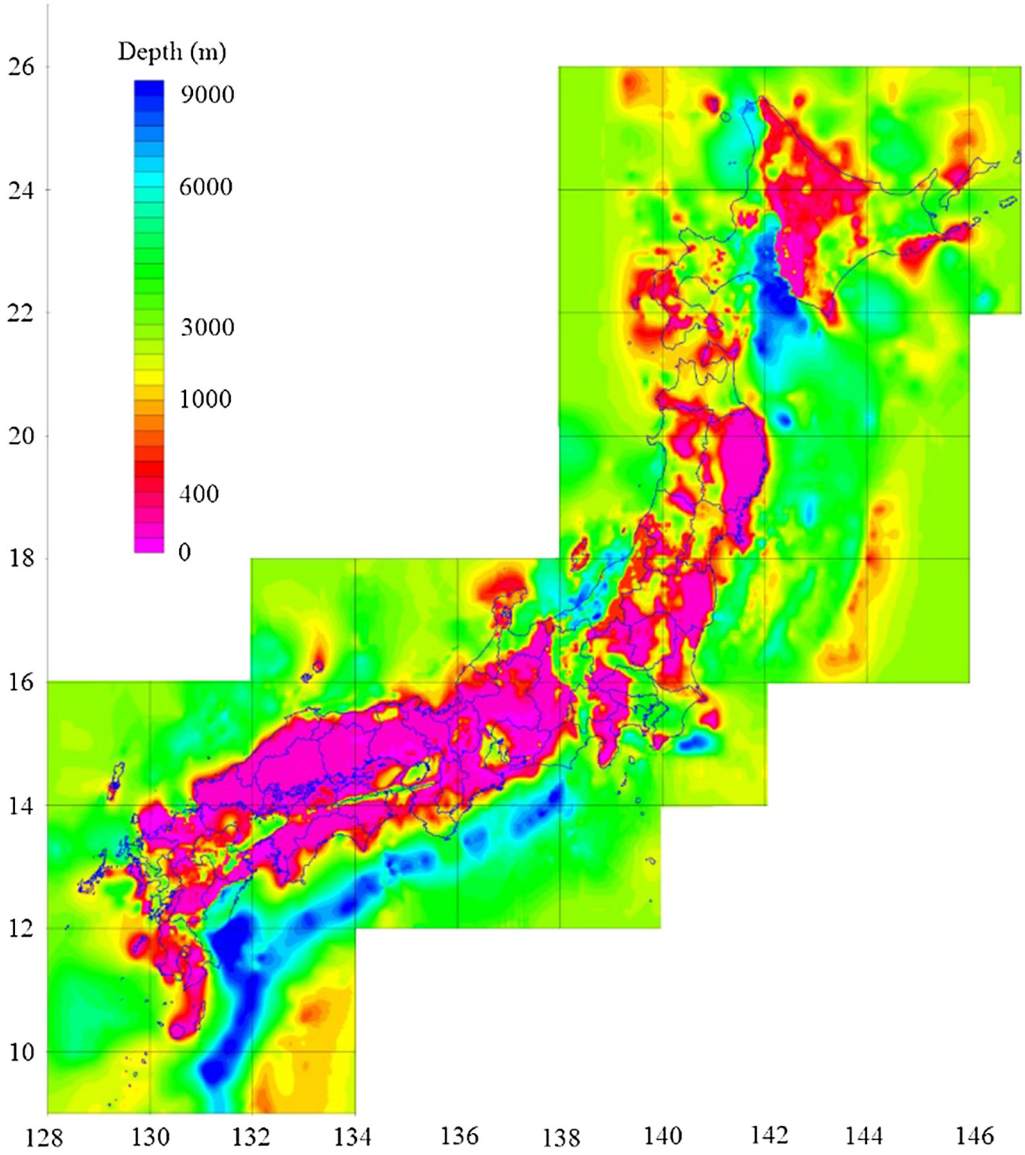

Figure 1. Topography of basement rock ($V_S = 3.0$ km/s) based on the Japan Seismic Hazard Information Station (J-SHIS) model (after Fujiwara *et al.*, 2009). The color version of this figure is available only in the electronic edition.

the theoretical horizontal-to-vertical spectral ratio (HVSR) curve to that of observed waveforms at each recording station. Ground-motion simulations were also carried out to confirm whether the proceeding modifications could lead to an improvement in reproducing observed ground shaking.

Table 1
Next Generation Attenuation-West2 Ground-Motion Models (GMMs)

GMM	Abbreviation	Zx*
Abrahamson *et al.* (2014)	ASK14	$Z_{1.0}$
Boore *et al.* (2014)	BSSA14	$Z_{1.0}$
Campbell and Bozorgnia (2014)	CB14	$Z_{2.5}$
Chiou and Youngs (2014)	CY14	$Z_{1.0}$

*Z_x depth to a shear-wave isosurface having $V_S = x$ km/s.

The first version of this structure model was published in 2009 (Fig. 1; Fujiwara *et al.*, 2009). Based on newly obtained data, the J-SHIS model was updated in 2012 (Fujiwara *et al.*, 2012).

The structure model consists of 33 layers, describing the upper, middle, and lower crustal structures. Each layer is assigned constant material properties, including *P*- and *S*-wave velocities (V_P, V_S), mass density (ρ), and quality factors (Q_P, Q_S). For instance, the shear-wave velocity of the first layer is 350 m/s, increasing monotonically to 3400 m/s of layer 33. The vertical configuration of these 33 layers varies with sites. In this study, we use the updated J-SHIS model (Fujiwara *et al.*, 2012), which better represents the state of the practice than the initial version, although the 2009 version was used in the NGA-West2 project. Extracted depths from the J-SHIS model are assigned a

Downloaded from https://pubs.geoscienceworld.org/ssa/bssa/article-pdf/doi/10.1785/0120190016/4832689/bssa-2019016.1.pdf
by GeoForschungsZentrums Potsdam, Chuanbin Zhu

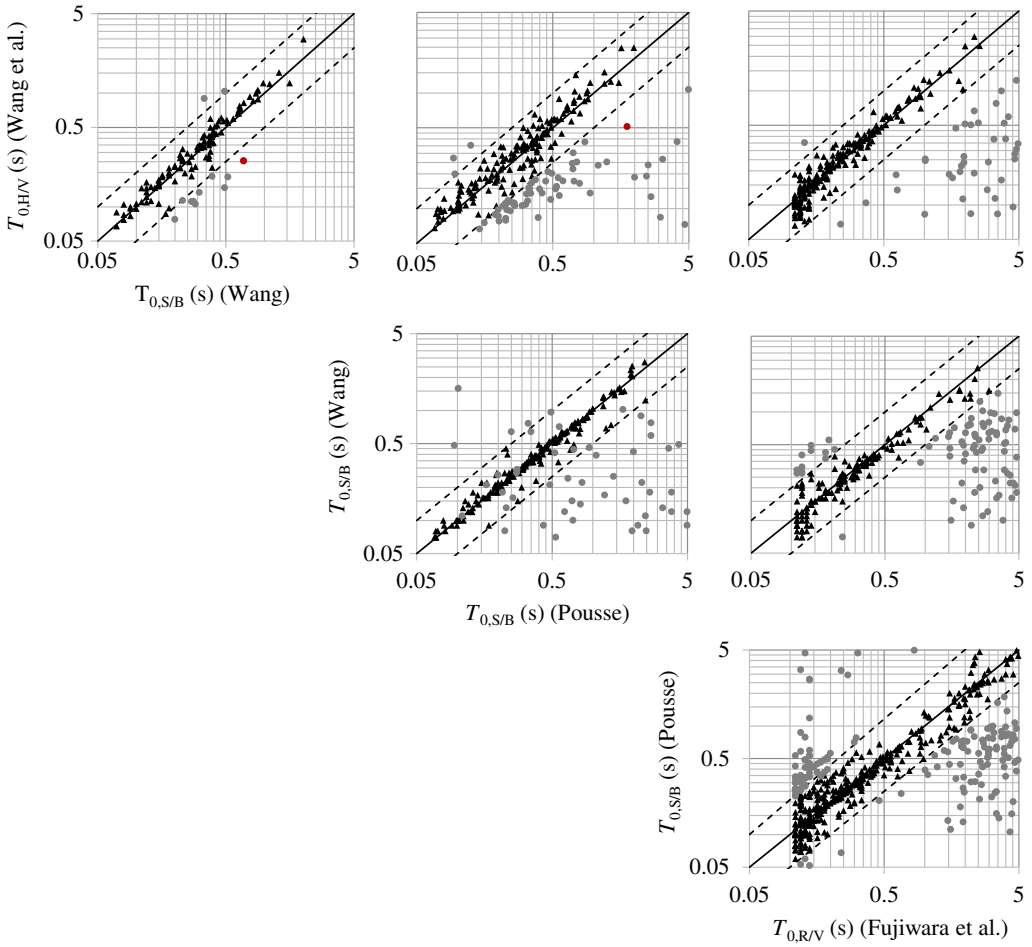

Figure 2. Consistency check on empirically derived site periods at KiK-net stations, Japan. The color version of this figure is available only in the electronic edition.

subscript "J-SHIS", that is, $Z_{x-\mathrm{J-SHIS}}$ (x = 0.8, 1.0, 1.5, and 2.5 km/s), to differentiate them from depths, Z_x, derived from *PS*-logging data.

Site-Specific Depth Measurements

KiK-net (Kiban Kyoshin network) is a strong-motion seismograph network that consists of ~700 recording stations across Japan (Okada *et al.*, 2004). Each station is equipped with a pair of seismographs with one on the ground surface and the other down a borehole. At most KiK-net stations, detailed surface-to-downhole *PS*-logging data are available, containing thickness, depth, *P*- and *S*-wave velocities (see Data and Resources). Thus, site-specific depth measurements can be established from the KiK-net 1D velocity profiles and then used as references to gauge the depth data extracted from the J-SHIS model ($Z_{x-\mathrm{J-SHIS}}$). But there is one prerequisite for this comparison to be trustworthy, which is that the KiK-net velocity profiles are robust enough to serve as a benchmark as discussed in several recent studies (e.g., Poggi *et al.*, 2012; Wu *et al.*, 2017; Pilz and Cotton, 2019). Therefore, before evaluating the J-SHIS model, we need to identify which KiK-net profiles are appropriate for such testing.

The usability of a velocity profile is judged based on the closeness of its fundamental resonant period (T_0) calculated using the profile to that derived using spectral ratio approaches on earthquake ground motions. To establish robust empirical data, we compiled four sets of T_0 for KiK-net sites (Fig. 2) in this investigation.

The first set of site period ($T_{0,\mathrm{H/V}}$) was derived by Wang *et al.* (2018) using horizontal-to-vertical (H/V) response (5%) spectral ratio on complete waveforms of earthquake recordings. Selected earthquake ground motions (at least 10 records per station) were recorded between January 2009 and July 2017 with moment magnitudes (M_w) > 3 and peak ground acceleration (PGA) ranging between 2 and 20 cm/s^2. Eventually, 265 (56%) of 473 sites (Fig. 2) were assigned a $T_{0,\mathrm{H/V}}$.

The second set of site period ($T_{0,\mathrm{S/B}}$) was obtained by Wang (2017) using surface-to-borehole (S/B) cross-spectral ratio on earthquake ground motions (at least five records per station) with PGA in the range between 5 and 20 cm/s^2. Spectral ratios were calculated on smoothed Fourier spectrum

Downloaded from https://pubs.geoscienceworld.org/ssa/bssa/article-pdf/doi/10.1785/0120190016/4832689/bssa-2019016.1.pdf
by GeoForschungsZentrums Potsdam, Chuanbin Zhu

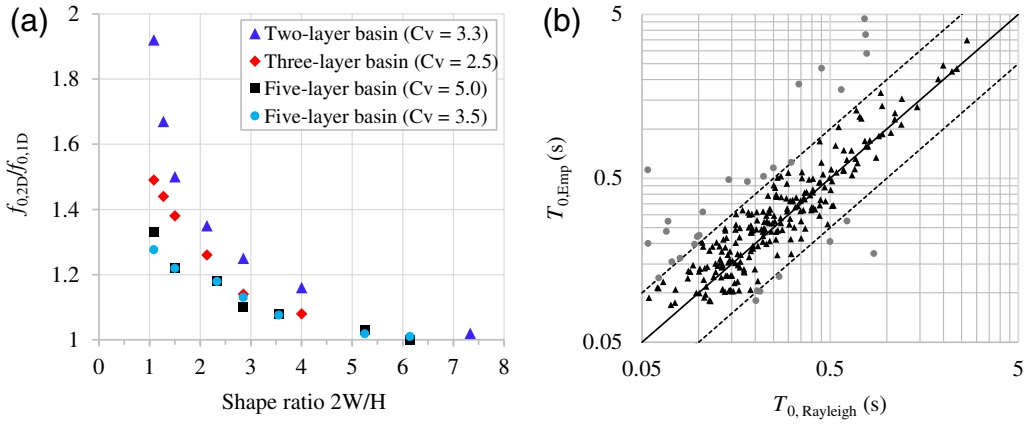

Figure 3. (a) Ratio of fundamental frequencies between 2D and 1D modeling (after Zhu *et al.*, 2017); Cv is the shear-wave velocity contrast between bedrock and sediment. (b) Comparison between empirically derived site periods using strong-motion records $T_{0,Emp}$ and analytically derived (Rayleigh) site periods using velocity profiles $T_{0,Rayleigh}$ at KiK-net stations, Japan. The color version of this figure is available only in the electronic edition.

of complete waveforms and then were corrected using the coherence between the signals recorded at the ground surface and downhole to account for the potential destructive interference at downhole sensors (Steidl *et al.*, 1996; Safak, 1997). $T_{0,S/B}$ could be clearly identified for 249 KiK-net sites (Fig. 2).

The third set of site period ($T_{0,S/B}$) was acquired by Pousse (2005) using S/B Fourier spectral ratio on complete waveforms of earthquake recordings. Selected ground motions were from earthquakes with hypocentral depths smaller than 25 km, hypocentral distances ranging between 0.5 and 343 km, moment magnitudes between 4.0 and 7.3, and PGAs between 0.4 and 927 cm/s^2. Finally, 538 KiK-net stations were assigned a $T_{0,S/B}$ (Fig. 2).

The last set of site period ($T_{0,R/V}$) was published by the NIED (Fujiwara *et al.*, 2009). $T_{0,R/V}$ corresponds to the first peak (from the long-period side) on the Fourier spectral ratios of *S*-coda waves (20 s after *S*-wave arrival) of the radial component to that of the vertical component (R/V). Hence, $T_{0,R/V}$ reflects the site response to Rayleigh waves more than to shear waves and is often used to calibrate subsurface velocity structure based on Rayleigh-wave ellipticity. All 673 KiK-net stations were assigned a $T_{0,R/V}$ (Fig. 2).

Because these empirical site periods were derived either by different teams or using distinct techniques, it is thus unavoidable that there will be a certain level of discrepancy. For example, site periods were defined to correspond to significant peaks on a spectral ratio curve, but what qualified a significant peak was defined subjectively, especially in cases of a spiky H/V curve. This discretionary exercise led to different levels of confidence in these four sets of site periods and partially contributed to the deviation of scatter points from the 1-to-1 line in Figure 2. Therefore, to guarantee the robustness of empirical data, we carried out a consistency check on these site periods.

We consider two site periods consistent if the ratio between them is in the range between 0.5 and 2.0. This range was also adopted by many other researchers (e.g., Cadet *et al.*, 2012; Pilz and Cotton, 2019). We first select sites with at least two entries (maximum, four) of site periods; there are 588 KiK-net sites fulfilling this criterion. Of these 588 stations, we then identify sites at which site periods are consistent with each other, that is, the ratio between any two site periods in the range between 0.5 and 2.0. Finally, there are 331 KiK-net sites passing the consistency check (Fig. 2). Site periods (number ≥ 2) at a site are then averaged, and the mean value is used as the empirical site period at the site.

The Rayleigh method is the most efficient and rigorous approach to approximate the value of the fundamental period from a given 1D soil profile with a varying velocity with depth (Dobry *et al.*, 1976). Thus, the Rayleigh method was implemented to calculate theoretical site periods using the equation

$$T_{0,\mathrm{Rayleigh}}=2\pi\sqrt{\left(\int_0^H \rho(z)X(z)^2dz\right)/\left(\int_0^H \rho(z)V_s(z)^2\left(\frac{dX(z)}{dz}\right)^2dz\right)},$$

in which $X(z)$ is the fundamental modal shape at elevation z, which is measured up from the bottom of the profile, and $\rho(z)$ and $V_S(z)$ are the mass density and shear-wave velocity, respectively, at z. The fundamental modal shape is estimated through iterations (e.g., Urzúa *et al.*, 2017).

The Rayleigh procedure is based on 1D assumption. Thus, if a site exhibits multidimensional features, its theoretical resonant period deviates from the period derived empirically, and the level of deviation depends on the extent to which the site is influenced by 2D or 3D effects. However, both theoretical and instrumental studies (e.g., Bard and Bouchon, 1985; Roten *et al.*, 2006; Zhu and Thambiratnam, 2016) show that lateral inhomogeneity does not alter fundamental period significantly, for example, in general, less than a factor of 2.0 for both 2D (Fig. 3a; Zhu *et al.*, 2017) and 3D sites (e.g., Woolery and Street, 2002). Thus, taking into account the prospective impact of lateral variation in velocities on site period, a 1D velocity profile is only deemed

Downloaded from https://pubs.geoscienceworld.org/ssa/bssa/article-pdf/doi/10.1785/0120190016/4832689/bssa-2019016.1.pdf
by GeoForschungsZentrums Potsdam, Chuanbin Zhu

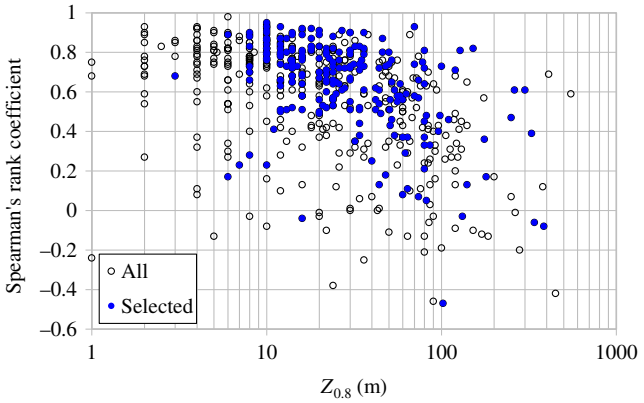

Figure 4. Spearman's rank correlation coefficient r versus site depth $Z_{0.8}$ for all KiK-net sites. Coefficients close to one indicate sites featuring a 1D site response. Site with 2D/3D characteristic are associated with lower values of the coefficient (Pilz and Cotton, 2019). The color version of this figure is available only in the electronic edition.

usable if its theoretical (fundamental) period is in the range of 0.5–2.0 times of its empirical site period. Among the 331 KiK-net sites, 229 (or 70%) profiles passed the usability check (Fig. 3b). Ⓔ Table S1 (available in the supplemental content to this article) contains the site information of these 229 KiK-net stations, and Ⓔ Figure S1 displays the spatial distribution of these stations. Poggi *et al.* (2012) found a similar number (220) of KiK-net profiles in which the theoretical site period matches its empirically derived one.

Under these stringent conditions (consistency and usability), the number of sites reduces from ~700 to 229. To examine whether our data selection procedure preferentially removes KiK-net sites featuring 2D or 3D responses, we take advantage of the results of our team's previous study. Pilz and Cotton (2019) systematically evaluated 2D or 3D site effects at KiK-net stations based on the closeness of the empirical amplification function to the theoretical transfer function at a given site. Empirical amplification functions were derived following an inversion procedure proposed by Edwards *et al.* (2013), and theoretical transfer functions were computed for vertically propagating *SH* waves using the Knopoff layer-matrix formulation (Knopoff, 1964). Spearman's rank correlation coefficient r (Spearman, 1904) was calculated between the two functions in the period band ranging from 0.04 s to T_0 and was then used to detect 2D or 3D sites. Whereas a coefficient r close to 1 indicates a 1D-type site, a low r-value suggests a site with prominent 2D or 3D characteristics (Pilz and Cotton, 2019). Figure 4 depicts the Spearman's coefficient against $Z_{0.8}$ for all KiK-net stations and these 229 sites selected in the present research.

In Figure 4, there exists a positive but rather weak correlation between the prominence of 2D or 3D effects and site depth $Z_{0.8}$. In addition, data distributions in Figure 4 indicate that our site selection criterion, that is, $0.5 < T_{0,\mathrm{Emp}}/T_{0,\mathrm{Rayleigh}} < 2.0$, does not disproportionally exclude 2D or 3D sites. This is mainly because, during the site selection, we factored into the implications of basins effects on site fundamental period (Fig. 3a). Thus, in the following evaluation of the subsurface model J-SHIS, we use these 229 KiK-net sites only. Site-specific depth measurements Z_x ($x = 0.8$, 1.0, 1.8, and 2.5 km/s) at these sites are obtained directly from their velocity profiles whenever x km/s is first reached. Histograms of Z_x are presented in Figure 5. Among the 229 usable sites, 224 profiles reach or penetrate 1.0 km/s horizon, and the number of depth data becomes smaller with the increase in x.

Testing J-SHIS Depths to 1.0 and 2.5 km/s Velocity Isosurfaces

Measured depth at each KiK-net station is compared with the depth extracted from the J-SHIS velocity model at the same location. The comparison is shown in Figure 6 for $x = 1.0$ and 2.5 km/s. Ideally, $Z_{x\mathrm{J\text{–}SHIS}}$ should be equal to Z_x at the same site. However, data points in Figure 6a are scattered in a broad area away from the one-to-one line, indicating deviations of $Z_{1.0\_\mathrm{J\text{–}SHIS}}$ from $Z_{1.0}$ to different extents. To quantify the comparison, we adopt one goodness-of-fit indicator, the Nash–Sutcliffe efficiency (NSE) coefficient (Nash and Sutcliffe, 1970). NSE can range from $-\infty$ to 1. Essentially, the closer the model efficiency is to 1, the better the match is. Threshold values indicating a good fit have been suggested between 0.5 and 0.65 (Ritter and Muñoz-Carpena, 2013). For $x = 1.0$ km/s, the NSE is −0.4, which indicates that the J-SHIS depth predictions are worse than the mean of depth measurements. Scatter points in Figure 6b appear to be less dispersive (NSE = 0.78), which may suggest a higher quality of $Z_{2.5\_\mathrm{J\text{–}SHIS}}$ than $Z_{1.0\_\mathrm{J\text{–}SHIS}}$ or that it is caused by a poorly representative $Z_{2.5}$ data sample (Fig. 5).

At each KiK-net site, the depth residual is defined as the difference between depths from its borehole measurement (Z_x) and from the J-SHIS model ($Z_{x\_\mathrm{J\text{–}SHIS}}$) in natural log space. Residuals are plotted against J-SHIS depths in Figure 7. Regressions to residuals are also displayed in each plot, as well as their coefficients of determination. For $x = 0.8$ km/s (Fig. 7a), the J-SHIS velocity model underestimates the depth to $V_S = 0.8$ km/s at sites with $Z_{0.8\_\mathrm{J\text{–}SHIS}} < 35$ m and overestimates it at sites with $Z_{0.8\_\mathrm{J\text{–}SHIS}} > 35$ m. For $x = 1.0$, 1.5, and 2.5 km/s (Fig. 7b–d), the crossovers are 43, 53, and 84 m, respectively. For a site with $Z_{1.0\_\mathrm{J\text{–}SHIS}} = 100$ m, according to the regression line in Figure 7b, namely, $\ln Z_{1.0} - \ln 100 = -0.77 \ln 100 + 2.89$ for this case, one could expect the actual depth $Z_{1.0}$ to be 51.89 m. J-SHIS depth is $100 - 51.89 = 48.11$ m larger than its measurement on average. Mean μ and standard deviation σ of residuals are also given in Figure 7.

When $Z_{x\_\mathrm{J\text{–}SHIS}}$ is relatively small, there is a positive depth difference ($\ln Z_x - \ln Z_{x\_\mathrm{J\text{–}SHIS}}$), which means that J-SHIS model tends to give depths smaller than measurements. In contrast, there exists a negative depth difference when $Z_{x\_\mathrm{J\text{–}SHIS}}$ is relatively large. Similar problems were also identified in the southern California basin model

Downloaded from https://pubs.geoscienceworld.org/ssa/bssa/article-pdf/doi/10.1785/0120190016/4832689/bssa-2019016.1.pdf
by GeoForschungsZentrums Potsdam, Chuanbin Zhu

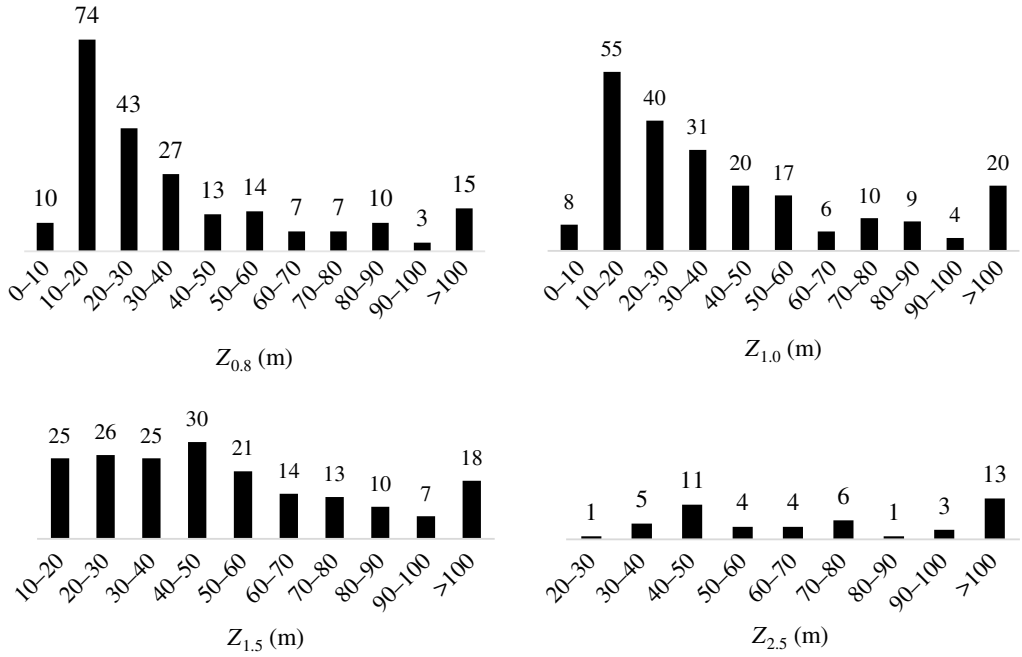

Figure 5. Histograms of depths $Z_{0.8}$, $Z_{1.0}$, $Z_{1.5}$, and $Z_{2.5}$ derived from KiK-net velocity profiles (*PS* logging). Total numbers of sites with $Z_{0.8}$, $Z_{1.0}$, $Z_{1.5}$, and $Z_{2.5}$ measurements are 224, 221, 190, and 49, respectively.

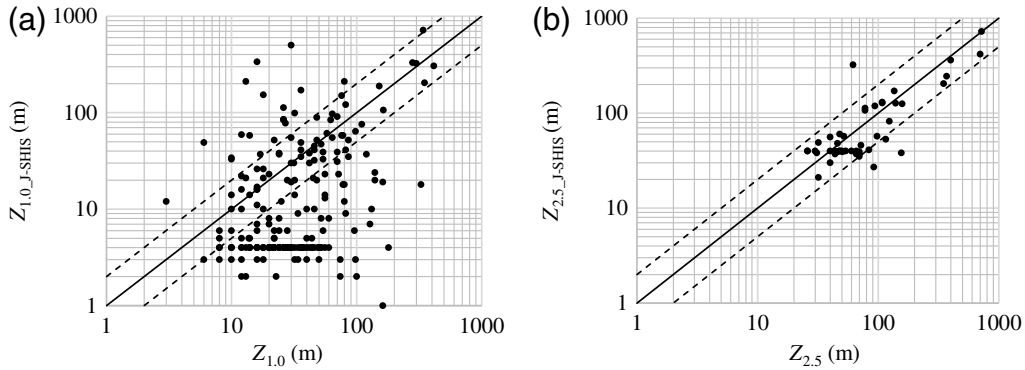

Figure 6. Comparison of depth data from borehole loggings versus those from the subsurface model J-SHIS at KiK-net sites in Japan for (a) $Z_{1.0}$ and (b) $Z_{2.5}$.

(Magistrale *et al.*, 2000) by Stewart *et al.* (2005). For the southern California basin model, the mean and standard deviation of residuals between inferred and measured $Z_{1.5}$ are 107 and 408 m, respectively, but they are 8.88 and 78.71 m for the J-SHIS model. The J-SHIS model seems to have a higher estimation accuracy of depth than the southern California basin model. This may be attributed to the fact that borehole loggings at many KiK-net stations extend to a very large depth (e.g., 216 boreholes deeper than 200 m), and these loggings were used in the velocity modeling to add constraints on the subsurface structure. However, thicknesses of sediments at each observation station were later modified during the tuning to match the peak period of theoretical HVSRs to that of ground-motion records. This modification may skew the J-SHIS depths from their initial values (measurements) at datum points.

Implications for NGA-West2 GMMs

The purpose of incorporating sedimentary depth into GMMs is to improve the estimate of relatively long-period ground motions, especially in large-scale urban basins, for example, the Los Angeles basin and the San Francisco basin in California, as well as the Kanto basin in Japan. In the NGA-West2 project, the J-SHIS 3D model was used to establish depth data for many recording stations in Japan (e.g., 71% of $Z_{1.0}$ data) where there were no site-specific measurements reaching the required shear-wave velocity. Based on both measured and inferred Z_x, correlation equations (e.g., CY14 and CB14) were proposed to relate Z_x to V_{S30}. These correlations were then utilized in some NGA-West2 GMMs (e.g., BSSA14) to estimate the average depth associated with V_{S30}, although the use of these relations was not without

Downloaded from https://pubs.geoscienceworld.org/ssa/bssa/article-pdf/doi/10.1785/0120190016/4832689/bssa-2019016.1.pdf
by GeoForschungsZentrums Potsdam, Chuanbin Zhu

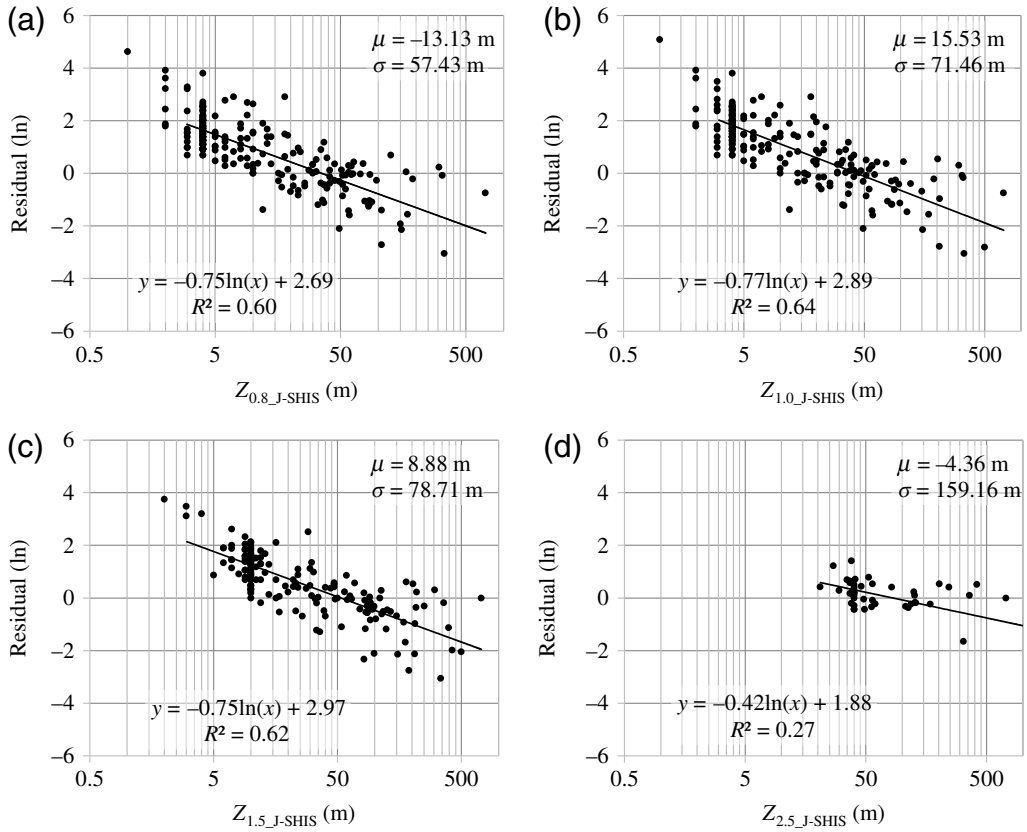

Figure 7. Residual between measured and inferred depth for (a) $Z_{0.8}$, (b) $Z_{1.0}$, (c) $Z_{1.5}$, and (d) $Z_{2.5}$ in natural log space. μ and σ are the mean and standard deviation of residuals, respectively; solid lines are regressions to residuals; R^2 is the coefficient of determination.

dispute. In this section, we evaluate the implications of inferred depths on the previously developed $Z_x - V_{S30}$ relations and on ground-motion estimation.

$Z_x - V_{S30}$ Centring

Based on both measured and the J-SHIS depth data in the NGA-West2 site database, CY14 proposed a correlation relationship to estimate the average or representative depth $\bar{Z}_{1.0}$ (unit: m) associated with V_{S30} (equation 1), for Japan. Likewise, CB14 developed an equation relating $\bar{Z}_{2.5}$ (unit: km) to V_{S30} (equation 2) for Japan:

$$\ln \bar{Z}_{10} = \frac{-5.23}{2} \ln\left(\frac{V_{S30}^2 + 412^2}{1360^2 + 412^2}\right) \quad (1)$$

$$\ln \bar{Z}_{2.5} = 5.359 - 1.102 \ln V_{S30}. \quad (2)$$

Both correlation relations display a high degree of scatter. For instance, the coefficient of determination of the $\bar{Z}_{2.5} - V_{S30}$ model (equation 2) is only 0.112, and the standard deviation of regression residuals is 1403 m. Apart from the known reason that it is inherently difficult to use such property of superficial soil layers as V_{S30} to infer subsurface velocity structure much deeper than 30 m (Kaklamanos and Baise, 2011), the incorporation of J-SHIS depth data in the dataset may also contribute to the poor correlation and large dispersion. The uncertainty in J-SHIS depth data, as shown in Figure 7, was inevitably mapped into these correlation equations.

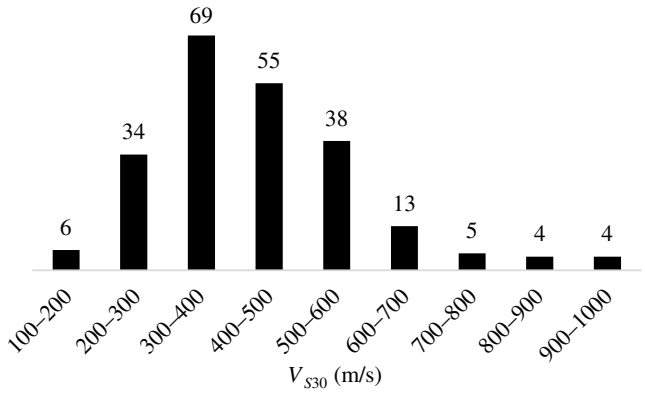

Figure 8. Histograms of V_{S30} (m/s) of 229 KiK-net sites considered having reliable velocity profiles.

We also obtained V_{S30} data for the 229 KiK-net sites that are considered as having usable velocity profiles. Because velocity models at these sites exceed 30 m, V_{S30} is calculated directly from borehole logging data by averaging velocities over the top 30 m. Figure 8 shows the histogram of V_{S30}. We then plot both measured and J-SHIS depth data, which are

Downloaded from https://pubs.geoscienceworld.org/ssa/bssa/article-pdf/doi/10.1785/0120190016/4832689/bssa-2019016.1.pdf
by GeoForschungsZentrums Potsdam, Chuanbin Zhu

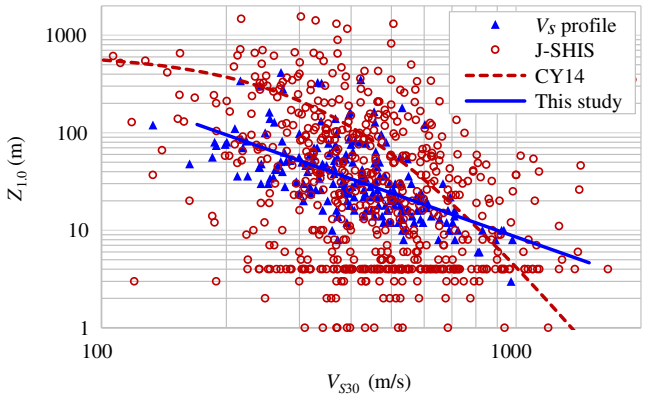

Figure 9. Site depth $Z_{1.0}$ from different sources versus shear-wave velocity V_{S30}. Solid and dashed lines represent regression models proposed in this study (equation 6) and by Chiou and Youngs (2014; hereafter, CY14) (equation 1), respectively, for Japan. The color version of this figure is available only in the electronic edition.

compiled independently in this study, against V_{S30} in Figure 9.

In Figure 9, V_{S30} exhibits certain linear correlation with measured depth to 1000 m/s. Thus, we exclude the J-SHIS depth data and only keep the depth measurements. Based completely on depth measurements, we then develop $\bar{Z}_x - V_{S30}$ correlation models in natural logarithm units, as shown in Figure 10, using the following functional form:

$$\ln \bar{Z}_x = c_0 + c_1 \ln V_{S30} \pm \sigma_{\mathrm{RES}}, \tag{3}$$

in which c_0 and c_1 are regression coefficients given in Figure 10 and σ_{RES} is the deviation of regression residuals and is defined as

$$\sigma_{\mathrm{RES}} = \sqrt{\frac{\sum_1^N (\ln Z_x - \ln[\bar{Z}_x(V_{S30})])^2}{N}}, \tag{4}$$

in which N is the total number of depth estimates.

F-statistics is performed to test the null hypothesis and shows that regression coefficients in each model are statistically significant at the 5% significance level. Other forms of predictor variable, for example, V_{S30} and $1/V_{S30}$, were also considered, but the $\ln V_{S30}$ performed best as a predictor variable. Second-order and higher order polynomial regressions were also tested but resulted in an insignificant increase in R^2, and thus we adopted the functional form of equation (3). In Figure 10a,b, $Z_{0.8}$ and $Z_{1.0}$ are moderately correlated with V_{S30} (in natural log space) with Pearson's correlation coefficient $r = 0.62$ (equivalent to R in this case), and thus both regression relationships for $\bar{Z}_{0.8}$ and $\bar{Z}_{1.0}$ (equations 5 and 6) have fairly large variabilities:

$$\ln \bar{Z}_{0.8} = 12.30 - 1.50 \ln V_{S30} \tag{5}$$

$$\ln \bar{Z}_{1.0} = 12.50 - 1.50 \ln V_{S30}. \tag{6}$$

Compared with $\bar{Z}_{0.8}$ and $\bar{Z}_{1.0}$, the correlations between V_{S30} and $\bar{Z}_{1.5}$ (Fig. 10c) and between V_{S30} and $\bar{Z}_{2.5}$ (Fig. 10d) are poorer as evidenced by the lower correlation coefficients. This may be attributed to the less representative $Z_{1.5}$ and $Z_{2.5}$ data samples, whereas $Z_{0.8}$ and $Z_{1.0}$ data approximately follow a lognormal distribution (Fig. 4). Regression equations for $\bar{Z}_{1.5}$ and $\bar{Z}_{2.5}$, in Figure 10c and 10d, respectively, are thus not given here. However, the poorer correlations might suggest that, for Japan, $Z_{1.5}$ and $Z_{2.5}$ are better site proxies than $Z_{0.8}$ and $Z_{1.0}$ in terms of capturing the remaining site effects that are not accounted for using V_{S30}.

In Figure 9, our $\bar{Z}_{1.0} - V_{S30}$ relation (equation 6) is compared with equation (1) (CY14). For V_{S30} below 800 m/s, equation (1) (CY14) gives higher $\bar{Z}_{1.0}$ estimates than equation (6) (this study). This is because CY14 fitted equation (1) to both the J-SHIS (>90 m) and measured depths. As illustrated in Figure 7, at deep sites, there are negative depth differences ($\ln Z_x - \ln Z_{x\_\mathrm{J-SHIS}}$). As a result, CY14's equation is also biased for deep sites.

Based on the measured depth dataset, we compared the prediction powers of the two correlation models (equations 1 and 6) using the NSE coefficient (Nash and Sutcliffe, 1970) which measures the goodness of fit of the depth measurements and estimates about the one-to-one line. The value of NSE for our model (equation 6) is 0.38, which is much higher than that of the CY14 model (equation 1), that is, −1.25, which suggests that the arithmetic mean of the observed values has greater prediction accuracy than the CY14 model. Although equation (6) is more descriptive of the measured depth data than equation (1) (CY14), both correlation relations have considerably large scatters with $\sigma_{\mathrm{RES}} = 0.68$ and 0.77, respectively.

The majority of measured depth data used in the present study comes from KiK-net stations, most of which are installed on weathered rocks or stiff soils with relatively thin overlays (Okada *et al.*, 2004). Thus, the $\bar{Z}_{1.0} - V_{S30}$ relation (equation 6) could potentially underestimate the depths for sites in sedimentary basins. To verify this, we identify recording stations (KiK-net and K-NET) in basins, including the Kanto, Osaka, Nagoya, and Sendai basins. Among them, 27 stations (Ⓔ Table S2) have velocity logging data reaching or exceeding 1.0 km/s, and thus only the site data (V_{S30} and $Z_{1.0}$) for these sites are displayed in Figure 11. Because there are not adequate recording stations located in deep basins, performances of two $\bar{Z}_{1.0} - V_{S30}$ equations (equations 1 and 6) cannot be evaluated in a statistically meaningful manner. However, Figure 11 demonstrates that our $\bar{Z}_{1.0} - V_{S30}$ model (equation 6) does not significantly underestimate the depth of basin sites and instead can represent the data trend (by visual inspection).

Ground-Motion Prediction

Basin effects have been accounted for in a number of empirical investigations by adding a depth parameter into GMMs and are dealt with either as a separate component

Downloaded from https://pubs.geoscienceworld.org/ssa/bssa/article-pdf/doi/10.1785/0120190016/4832689/bssa-2019016.1.pdf
by GeoForschungsZentrums Potsdam, Chuanbin Zhu

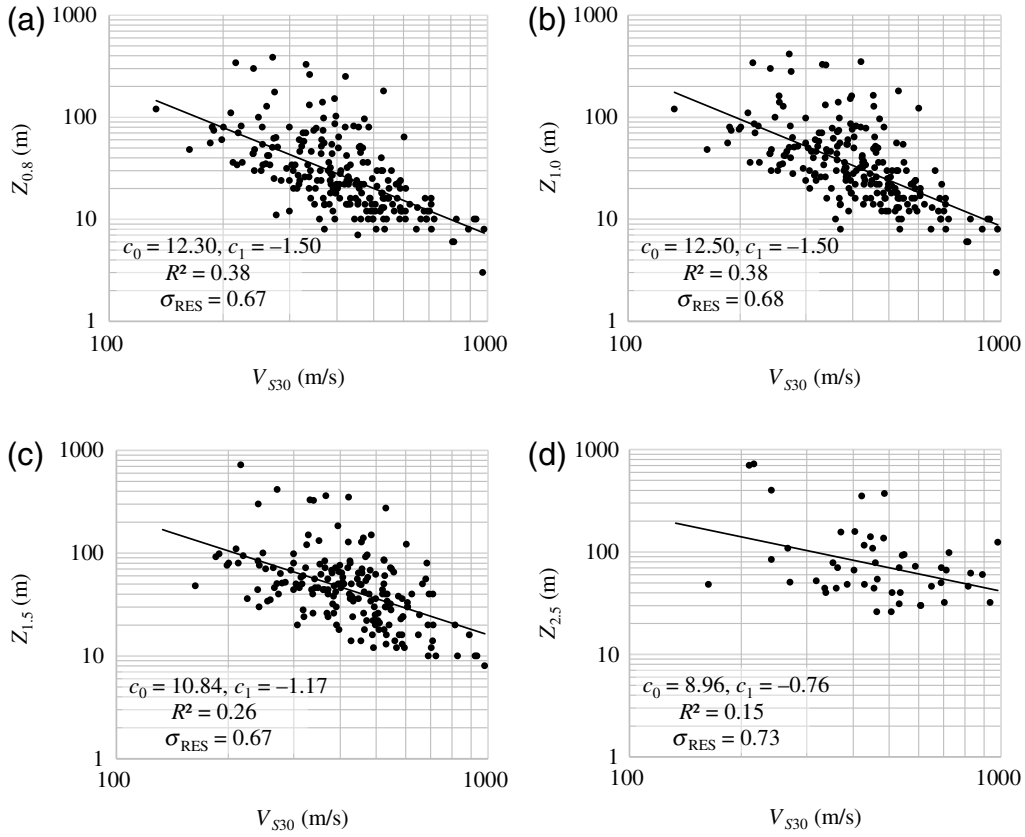

Figure 10. Measured depths (a) $Z_{0.8}$, (b) $Z_{1.0}$, (c) $Z_{1.5}$, and (d) $Z_{2.5}$ versus shear-wave velocity V_{S30}. Straight lines represent regressions to the data in each figure; R^2 is the coefficient of determination; σ_{RES} is the deviation of regression residuals as defined in equation (4).

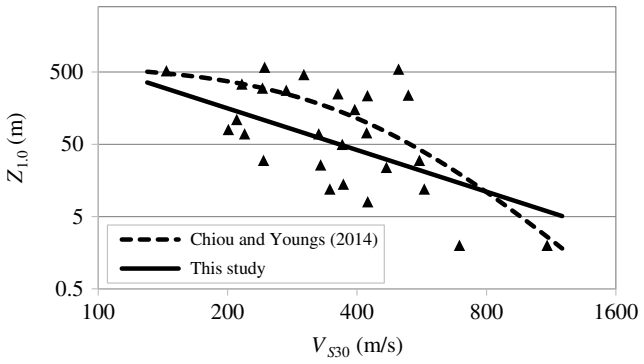

Figure 11. Measured depth $Z_{1.0}$ versus V_{S30} for recording stations in the Kanto, Osaka, Nagoya, and Sendai basins. Solid and dashed lines represent the $Z_{1.0} - V_{S30}$ models proposed in this study (equation 6) and that by CY14 (equation 1), respectively.

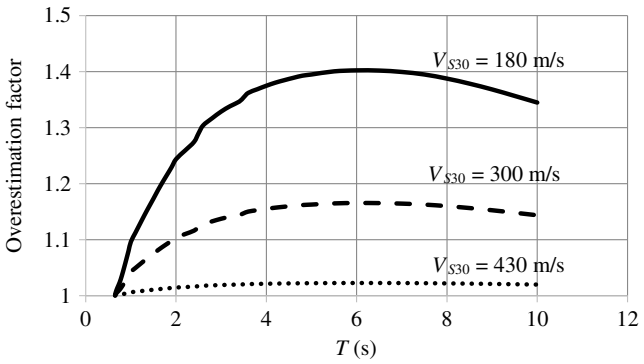

Figure 12. Overestimation bias in ground motion caused by the bias in depth estimate at a site with $Z_{1.0\_J-SHIS} = 100$ m using the Boore *et al.* (2014) model.

to be plugged into an existing GMM (e.g., Choi *et al.*, 2005) or as an integral part of a GMM (e.g., NGA-West2 models). BSSA14 introduces $Z_{1.0}$ into their GMM as follows:

$$F(\delta Z_{1.0}) = \begin{cases} 0 & T < 0.65 \\ f_6 \delta Z_{1.0} & T \geq 0.65 \text{ and } \delta Z_{1.0} \leq f_7/f_6 \\ f_7 & T \geq 0.65 \text{ and } \delta Z_{1.0} > f_7/f_6 \end{cases} \quad (7)$$

$$\delta Z_{1.0} = Z_{1.0} - \bar{Z}_{1.0}, \quad (8)$$

in which $F(\delta Z_{1.0})$ is the depth-related amplification in natural log units; f_6 and f_7 are period-dependent regression coefficients; and $\delta Z_{1.0}$ is the depth difference between $Z_{1.0}$ and $\bar{Z}_{1.0}$, in which $\bar{Z}_{1.0}$ is the representative depth associated with V_{S30} and is estimated using equation (1) (CY14). For $T \geq 0.65$ s and $Z_{1.0} \leq f_7/f_6$, BSSA14 models, the

Downloaded from https://pubs.geoscienceworld.org/ssa/bssa/article-pdf/doi/10.1785/0120190016/4832689/bssa-2019016.1.pdf
by GeoForschungsZentrums Potsdam, Chuanbin Zhu

depth-dependent amplification as a linear function of the depth difference $\delta Z_{1.0}$.

Besides the difference between J-SHIS depths and measurements (Fig. 7), there is also a difference between estimates of average depth using equation (1) (CY14, based primarily on J-SHIS depths) and equation (6) (this study, based completely on depth measurements), as shown in Figure 9. To evaluate the implications of the differences in both depths on ground-motion estimation, we take a site with $V_{S30} = 180$ m/s and $Z_{1.0\_\text{J-SHIS}} = 100$ m as an example. For such a site with $Z_{1.0\_\text{J-SHIS}} = 100$ m, one could expect an overestimation bias of ~48 m in $Z_{1.0\_\text{J-SHIS}}$ according to the regression line in Figure 7b. For a site with $V_{S30} = 180$ m/s, there would be an overestimation bias of ~298 m in the average depth according to the comparison between equations (1) (CY14) and (6) (this study) in Figure 9. Then, the bias in depth difference $\delta Z_{1.0}$ can be obtained using equation (8) to be 250 m, and then the consequent bias in basin amplification at various periods (>0.65 s) can be estimated using equation (7), as shown in Figure 12.

Figure 12 illustrates that, for such a site with $V_{S30} = 180$ m/s, basin amplification at oscillator period 1.0 s could be overestimated by a factor of 1.1, and this factor would increase gradually to 1.4 at period 6.0 s. For periods higher than 1.7 s, the overestimation factor is above 1.2, which could have a significant impact on ground-motion prediction. However, the overestimation factor decreases with V_{S30}. For example, the overestimation factor is no more than 1.17 for $V_{S30} = 300$ m/s and is negligible for $V_{S30} = 430$ m/s (Fig. 12). If the depth parameter for a site of interest is obtained from the J-SHIS model, the bias described should be included in the standard error of the BSSA14. However, one should caution the use of other sources of depth data when implementing NGA-West2 GMMs.

Discussion and Conclusions

The NGA-West2 project assigned the depths extracted from the J-SHIS subsurface structure model to many recording stations in Japan. After comparing the J-SHIS depths with their corresponding depth measurements derived from selected KiK-net velocity profiles, we find that the J-SHIS model underestimates site depths at shallow sites and overestimates depths at deep sites. Stewart *et al.* (2005) reported similar results with the southern California basin model (Magistrale *et al.*, 2000). The difference between J-SHIS estimates and measurements (*PS* logging) can result in a significant overestimation of ground motions, especially at soft sites, using BSSA14. Another two NGA-West2 GMMs, ASK14 and CY14, also use $Z_{1.0}$ and the $\bar{Z}_{1.0} - V_{S30}$ correlation equation proposed by CY14 and thus might have similar issues as BSSA14. Although this difference should be incorporated in NGA-West2 GMMs, one should caution the use of depth data from sources other than the J-SHIS model when implementing the NGA-West2 GMMs for sites in Japan. However, this depth-related estimation error can be reduced or eliminated by utilizing an alternative site characterizing proxy, for instance, site resonant period (or frequency). Site period should be considered for two main reasons.

Table 2
Identification of Site Frequency Using the Horizontal-to-Vertical Spectral Ratio Approach

References	Recording Network	Percentage
Hassani and Atkinson (2018)	California	554 (72%) out of 767 sites
Hassani and Atkinson (2016)	CENA	315 (59%) out of 535 sites
Wang *et al.* (2018)	KiK-net	265 (56%) out of 473 sites
Kwak *et al.* (2017)	KiK-net and K-NET	1608 (97%) out of 1658 sites
Ghofrani *et al.* (2013)	KiK-net	Single "peak" (60%); two peaks (20%)
Fujiwara *et al.* (2009)	KiK-net	674 (100%) sites

CENA, central and eastern North America.

First, there is a consensus that resonant period can be reliably determined for many sites using the HVSR technique on either earthquake ground-motion recordings or ambient noises. One may argue that many sites do not have a clear site period, but the same is also true for site depth. In fact, site period is more attainable than site depth. As shown in Table 2, site period can be clearly identified for the vast majority of stations in a recording network using HVSR. In contrast, site depth is missing at many recording sites. For instance, in the NGA-West1 site database, only 710 (or 27%) of 2675 stations had a $Z_{1.0}$. Although the availability of the $Z_{1.0}$ was improved in the NGA-West2 project, there were only ~66% of stations having $Z_{1.0}$. Among these available depth data, only 10% were derived from measurements with the remaining 56% being inferred from regional velocity models (Ancheta *et al.*, 2014). The availability of measured $Z_{1.0}$ and $Z_{2.5}$ have not been significantly improved in the NGA-subduction site database (e.g., Ahdi *et al.*, 2017).

In addition to engineering utility, many investigations (e.g., Cadet *et al.*, 2012; C. Zhu *et al.*, unpublished manuscript, 2019, see Data and Resources) have consistently shown that site period has a better performance in depicting the residual amplification after V_{S30} scaling than measured depths, let alone inferred ones that have been shown to have large differences from their measured counterparts in this study and that by Stewart *et al.* (2005). Therefore, in terms of both performance and engineering utility, site period is preferable to site depth as a parameter complementing V_{S30}.

In summary, the J-SHIS model underestimates the site depths at shallow sites and overestimates the depths at deep sites. This can result in NGA-West2 GMMs giving significantly biased ground-motion estimation, especially at soft sites, if depth data are extracted from sources other than the J-SHIS velocity model. Besides the depth to a velocity horizon, site period should be considered to complement V_{S30} in depicting site effects.

Downloaded from https://pubs.geoscienceworld.org/ssa/bssa/article-pdf/doi/10.1785/0120190016/4832689/bssa-2019016.1.pdf
by GeoForschungsZentrums Potsdam, Chuanbin Zhu

Data and Resources

Velocity profiles of KiK-net and K-NET recording stations were downloaded from the http://www.kyoshin.bosai.go.jp (last accessed June 2018). The Japan Seismic Hazard Information Station (J-SHIS) velocity model was downloaded from http://www.j-shis.bosai.go.jp/map/?lang=en (last accessed June 2018). Supplemental content includes a table of site information (latitude, longitude, altitude, V_{S30}, and site period) of 229 KiK-net stations selected in this study, a figure of the spatial distribution of these 229 stations, and a table of K-NET and KiK-net stations with measured $Z_{1.0}$ in basins. The unpublished manuscript by C. Zhu, F. Cotton, and M. Pilz (2019), "Which is a better proxy, site period or depth to bedrock, in modelling linear site response in addition to the average shear-wave velocity?" submitted to *Bull. Earthq. Eng.*

Acknowledgments

The authors warmly thank the National Research Institute for Earth Science and Disaster Prevention (NIED), Japan, for making the high-quality KiK-net site data and the Japan Seismic Hazard Information Station (J-SHIS) velocity model easily accessible to the public. The first author thanks David M. Boore for providing the V_{S30} data at KiK-net stations, Yu Miao and Suyang Wang for providing site-period data, Zhandogn Su for numerous discussions, and Graeme Weatherill for proofreading. The suggestions of Associate Editor Sheri Molnar have been highly stimulating and have for example motivated the tests shown in Figure 4. The authors also thank the very constructive feedback from two anonymous reviewers. Part of the work was done when the first author was visiting the Earthquake Research Institute (ERI), University of Tokyo (host: Takashi Furumura). This work is supported by the Seismology and Earthquake Engineering Research Infrastructure Alliance for Europe (SERA) project funded by the EU Horizon 2020 Programme under Grant Agreement Number 730900.

References

Abrahamson, N. A., W. J. Silva, and R. Kamai (2014). Summary of the Abrahamson, Silva, and Kamai NGA-West2 ground-motion relations for active crustal regions, *Earthq. Spectra* **30,** 1025–1055.

Ahdi, S. K., T. D. Ancheta, V. Contreras, T. Kishida, D. Y. Kwak, A. O. Kwok, G. A. Parker, Y. Bozorgnia, and J. P. Stewart (2017). NGA-subduction site database, *16th World Conf. on Earthquake Engineering*, Santiago, Chile, 09–13 January 2017.

Ancheta, T. D., R. B. Darragh, J. P. Stewart, E. Seyhan, W. J. Silva, B. S.-J. Chiou, K. E. Wooddell, R. W. Graves, A. R. Kottke, D. M. Boore, *et al.* (2014). NGA-West2 database, *Earthq. Spectra* **30,** 989–1005.

Bard, P. Y., and M. Bouchon (1985). The two-dimensional resonance of sediment-filled valleys, *Bull. Seismol. Soc. Am.* **75,** 519–541.

Boatwright, J., L. Blair, R. Catchings, M. Goldman, F. Perosi, and C. Steedman (2004). Using twelve years of USGS refraction lines to calibrate the Brocher and others (1997) 3-D velocity model of the bay area, *U.S. Geol. Surv. Open-File Rept. 2004-1282*, Washington, D.C.

Boore, D. M., J. P. Stewart, E. Seyhan, and G. M. Atkinson (2014). NGA-West2 equations for predicting PGA, PGV, and 5% damped PSA for shallow crustal earthquakes, *Earthq. Spectra* **30,** 1057–1085.

Cadet, H., P. Y. Bard, A. M. Duval, and E. Bertrand (2012). Site effect assessment using KiK-net data: Part 2—Site amplification prediction equation based on f_0 and V_{sz}, *Bull. Earthq. Eng.* **10,** 451–489.

Campbell, K. W., and Y. Bozorgnia (2014). NGA-West2 ground motion model for the average horizontal components of PGA, PGV, and 5%-damped linear response spectra, *Earthq. Spectra* **30,** 1087–1115.

Chiou, B. S.-J., and R. R. Youngs (2014). Update of the Chiou and Youngs NGA ground motion model for average horizontal component of peak ground motion and response spectra, *Earthq. Spectra* **30,** 1117–1153.

Choi, Y., J. P. Stewart, and R. W. Graves (2005). Empirical model for basin effects accounts for basin depth and source location, *Bull. Seismol. Soc. Am.* **95,** 1412–1427.

Dobry, R., I. Oweis, and A. Urzua (1976). Simplified procedures for estimating the fundamental period of a soil profile, *Bull. Seismol. Soc. Am.* **66,** 1293–1321.

Douglas, J. (2011). Ground-motion prediction equations 1964–2010, *PEER Report 2011/102*, Pacific Earthquake Engineering Research Center, University of California, Berkeley.

Edwards, B., C. Michel, V. Poggi, and D. Fäh (2013). Determination of site amplification from regional seismicity: Application to the Swiss national seismic Networks, *Seismol. Res. Lett.* **84,** 611–621.

Fujiwara, H., S. Kawai, S. Aoi, N. Morikawa, S. Senna, H. Azuma, M. Ooi, K. X. Hao, N. Hasegawa, T. Maeda, *et al.* (2012). Some improvements of seismic hazard assessment based on the 2011 Tohoku earthquake, *Technical Note of the National Research Institute for Earth Science and Disaster Prevention*, Number 379.

Fujiwara, H., S. Kawai, S. Aoi, N. Morikawa, S. Senna, N. Kudo, M. Ooi, K. X. Hao, Y. Hayakawa, N. Yoyama, *et al.* (2009). A study on subsurface structure model for deep sedimentary layers of Japan for strong-motion evaluation, *Technical Note of the National Research Institute for Earth Science and Disaster Prevention*, Number 337.

Ghofrani, H., G. M. Atkinson, and K. Goda (2013). Implications of the 2011 M9.0 Tohoku Japan earthquake for the treatment of site effects in large earthquakes, *Bull. Earthq. Eng.* **11,** 171–203.

Graves, R. W., and B. T. Aagaard (2011). Testing long-period ground-motion simulations of scenario earthquakes using the M_w 7.2 El Mayor–Cucapah Mainshock: Evaluation of finite-fault rupture characterization and 3D seismic velocity models, *Bull. Seismol. Soc. Am.* **101,** 895–907.

Hassani, B., and G. M. Atkinson (2016). Applicability of the site fundamental frequency as a V_{S30} proxy for Central and Eastern North America, *Bull. Seismol. Soc. Am.* **106,** 653–664.

Hassani, B., and G. M. Atkinson (2018). Application of a site-effects model based on peak frequency and average shear-wave velocity to California, *Bull. Seismol. Soc. Am.* **108,** 351–357.

Kaklamanos, J., and L. G. Baise (2011). Model validations and comparisons of the Next Generation Attenuation of ground motions (NGA-West) project, *Bull. Seismol. Soc. Am.* **101,** 160–175.

Knopoff, L. (1964). A matrix method for elastic wave problems, *Bull. Seismol. Soc. Am.* **54,** 431–438.

Kwak, D. Y., J. P. Stewart, S. J. Mandokhail, and D. Park (2017). Supplementing V_{S30} with H/V spectral ratios for predicting site effects, *Bull. Seismol. Soc. Am.* **107,** 2028–2042.

Magistrale, H., S. Day, R. Clayton, and R. W. Graves (2000). The SCEC Southern California reference three-dimensional seismic velocity model version 2, *Bull. Seismol. Soc. Am.* **90,** S65–S76.

Nash, J. E., and J. V. Sutcliffe (1970). River flow forecasting through conceptual models: Part I, a discussion of principles, *J. Hydrol.* **10,** 282–290.

Okada, Y., K. Kasahara, S. Hori, K. Obara, S. Sekiguchi, H. Fujiwara, and A. Yamamoto (2004). Recent progress of seismic observation networks in Japan-Hi-net, F-net, K-NET and KiK-net, *Earth Planets Space* **56,** xv–xxviii.

Pilz, M., and F. Cotton (2019). Does the 1D assumption hold for site response analysis? A study of seismic site responses and implication for ground motion assessment using KiK-net strong-motion data, *Earthq. Spectra* **2,** 883–905.

Pitilakis, K., E. Riga, and A. Anastasiadis (2013). New code site classification, amplification factors and normalized response spectra based on a worldwide ground-motion database, *Bull. Earthq. Eng.* **11,** 925, doi: 10.1007/s10518-013-9429-4.

Poggi, V., B. Edwards, and D. Fäh (2012). Characterizing the vertical-to-horizontal ratio of ground motion at soft-sediment sites, *Bull. Seismol. Soc. Am.* **102,** 2741–2756.

Downloaded from https://pubs.geoscienceworld.org/ssa/bssa/article-pdf/doi/10.1785/0120190016/4832689/bssa-2019016.1.pdf
by GeoForschungsZentrums Potsdam, Chuanbin Zhu

Pousse, G. (2005). Analysis of K-NET and KiK-net data: Implications for ground motion prediction–acceleration time histories, response spectra and nonlinear site response, *Doctorate Thesis*, Joseph Fourier University Grenoble I.

Ritter, A., and R. Muñoz-Carpena (2013). Performance evaluation of hydrological models: Statistical significance for reducing subjectivity in goodness-of-fit assessments, *J. Hydrol.* **480,** 33–45.

Roten, D., D. Fah, C. Cornou, and D. Giardini (2006). Two-dimensional resonances in Alpine valleys identified from ambient vibration wavefields, *Geophys. J. Int.* **165,** 889–905.

Safak, E. (1997). Models and methods to characterize site amplification from a pair of records, *Earthq. Spectra* **13,** 97–129.

Spearman, C. (1904). The proof and measurement of association between two things, *Am. J. Psychol.* **15,** 72–101.

Steidl, J. H., A. G. Tumarkin, and R. J. Archuleta (1996). What is a reference site? *Bull. Seismol. Soc. Am.* **86,** 1733–1748.

Stewart, J. P., Y. Choi, R. W. Graves, and J. H. Shaw (2005). Uncertainty of southern California basin depth parameters, *Bull. Seismol. Soc. Am.* **95,** 1988–1993.

Süss, M. P., and J. H. Shaw (2003). P wave seismic velocity structure derived from sonic logs and industry reflection data in the Los Angeles basin, California, *J. Geophys. Res.* **108,** no. B3, Article Number 2170.

Urzúa, A., R. Dobry, and J. T. Christian (2017). Is harmonic averaging of shear wave velocity or the simplified Rayleigh method appropriate to estimate the period of a soil profile? *Earthq. Spectra* **33,** 895–915.

Wang, S. Y (2017). Study on site effect using ground motion data from KiK-net in Japan, *Doctoral Dissertation*, Institute of Engineering Mechanics, China Earthquake Administration, Harbin, China.

Wang, S. Y, Y. Shi, W. P. Jiang, E. L. Yao, and Y. Miao (2018). Estimating site fundamental period from shear-wave velocity profile, *Bull. Seismol. Soc. Am.* **108,** 3431–3445.

Woolery, E. W., and R. Street (2002). 3D near-surface soil response from H/V ambient-noise ratios, *Soil Dynam. Earthq. Eng.* **22,** 865–876.

Wu, H., K. Masaki, K. Irikura, and F. J. Sanchez-Sesma (2017). Application of a simplified calculation for full-wave microtremor H/V spectral ratio based on the diffuse field approximation to identify underground velocity structures, *Earth Planets Space* **69,** 162.

Zhu, C., and D. Thambiratnam (2016). Interaction of geometry and mechanical property of trapezoidal sedimentary basins with incident *SH* waves, *Bull. Earthq. Eng.* **14,** 2977–3002.

Zhu, C., D. Thambiratnam, and C. Gallage (2017). Inherent characteristics of 2D alluvial formations subjected to in-plane motion, motion, *J. Earthq. Eng.* doi: 10.1080/13632469.2017.1387199.

Helmholtz Centre Potsdam
GFZ German Research Centre for Geosciences
Telegrafenberg
14473 Potsdam, Germany
chuanbin@gfz-potsdam.de
pilz@gfz-potsdam.de
fcotton@gfz-potsdam.de

Manuscript received 30 January 2019;
Published Online 24 September 2019

Downloaded from https://pubs.geoscienceworld.org/ssa/bssa/article-pdf/doi/10.1785/0120190016/4832689/bssa-2019016.1.pdf
by GeoForschungsZentrums Potsdam, Chuanbin Zhu